EARLY PICOSECOND EVENTS IN THE PHOTOCYCLE OF BACTERIORHODOPSIN

H.-J. POLLAND,* M. A. FRANZ,* W. ZINTH,* W. KAISER,* E. KÖLLING,‡ AND D. OESTERHELT‡
*Physik Department E II der Technischen Universität München, München, Germany; and
‡Max-Planck-Institut für Biochemie, Martinsried b. München, Germany

ABSTRACT The primary processes of the photochemical cycle of light-adapted bacteriorhodopsin (BR) were studied by various experimental techniques with a time resolution of 5×10^{-13} s. The following results were obtained. (*a*) After optical excitation the first excited singlet state S_1 of bacteriorhodopsin is observed via its fluorescence and absorption properties. The population of the excited singlet state decays with a lifetime τ_1 of ~0.7 ps (430 ± 50 fs) (52). (*b*) With the same time constant the first ground-state intermediate *J* builds up. Its absorption spectrum is red-shifted relative to the spectrum of BR by ~30 nm. (*c*) The second photoproduct *K*, which appears with a time constant of $\tau_2 = 5$ ps shows a red-shift of 20 nm, relative to the peak of BR. Its absorption remains constant for the observation time of 300 ps. (*d*) Upon suspending bacteriorhodopsin in D_2O and deuterating the retinal Schiff base at its nitrogen (lysine 216), the same photoproducts *J* and *K* are observed. The relaxation time constants τ_1 and τ_2 remain unchanged upon deuteration within the experimental accuracy of 20%.

INTRODUCTION

Photosynthesis in halobacteria is based on bacteriorhodopsin's (BR) action as a light driven proton pump. The biochemistry, the biophysics, and the photochemistry of BR have been subject of intensive investigation (1).

In the cell membrane of *Halobacterium halobium*, BR forms a two-dimensional hexagonal lattice (the purple membrane), where three BR molecules are close enough to form excitonically coupled trimers. BR contains 248 amino acids and one chromophore, the retinal molecule, which is bound to lysine 216 via a protonated Schiff base. Retinal in BR occurs in two configurations: the light-adapted state is an all-*trans* configuration and has *trans* (or anti) configuration at the *C=N* (15, 16) double bond (2). This state is active in proton pumping. Upon extended incubation in the dark part of the molecules convert into a 13-*cis*, 15-*cis* (or syn) configuration (3), which is inactive in proton pumping.

Light absorption substantially changes the optical properties of bacteriorhodopsin, indicating a series of reactions of the retinal chromophore within the protein matrix. Excitation of the light-adapted BR starts an optical cycle (photocycle) with several intermediates named *J*, *K*, *L*, *M*, and *O*. They are characterized by their different absorption properties (4, 5). The cycle is completed within 10 ms at room temperature, returning the system to its initial form. The first intermediates store sufficient energy to mediate the active proton transport and to drive the system back to its initial state. The absorption changes during the photocycle are caused by configurational changes of the retinal chromophore and by deprotonation and subsequent reprotonation of the nitrogen atom at the Schiff base (1). Light-adapted BR contains the retinal in the all-*trans* form, whereas the early photoproduct *K* formed within several picoseconds and stable for ~1.5 μs was reported to contain the isomerized 13-*cis* retinal (6–8). Picosecond studies of BR containing a modified retinal (9, 12-phenylretinal) strongly suggest isomerization of the native BR in the very early steps (9). On the other hand, the deprotonation of the Schiff base appears to be a much slower process. In the state *K* the Schiff base is still protonated (10). Only 50 ms after excitation, during the formation of the intermediate *M*, the Schiff base loses its proton (11).

Of special interest are the very first events of the photocycle, where—during the formation of the intermediate *J* and *K*—the optical energy is stored in the BR molecules. Several publications have addressed the primary events (12–20). Time resolved fluorescence and absorption techniques have been employed. Unfortunately, the results were not unambiguous. (*a*) The fluorescence lifetime of BR was measured to be 15 ps (13) or <2 ps (20). (*b*) The formation time of state *K* was said to be 1 ps (18) and 11 ps (16). (*c*) Upon deuteration of the Schiff base an isotope effect of 1.6 for the rise time of the intermediate *K* was reported (16). The latter is difficult to reconcile with the fact that the Schiff base is protonated in BR as well as in the intermediates *J* and *K*.

In view of this situation we performed experiments searching for a consistent picture of the early events of the photocycle in bacteriorhodopsin. We report on time-resolved picosecond investigations of the emission and absorption properties of BR. The laser excitation/detection system used allowed excitation by single pulses with

low repetition rate and at low intensities. This avoids possible excitation of BR into higher lying states and rules out interference of photoproducts. The time resolution of 0.5 ps was sufficient to study the first excitated singlet state of BR and the first two intermediates J and K. Our experimental results provide a first complete and consistent description of the primary photochemical events in BR.

GLOSSARY

- A absorbance
- ΔA absorbance change induced by the exciting pulse
- BR Bacteriorhodopsin in the purple membrane
- BR^*_{mon} excited BR, the excitation energy is localized on one monomer of the BR trimer
- BR_{s1} BR in the excited singlet state S_1
- D dichroitic ratio
- d-BR Bacteriorhodopsin in D_2O; a hydrogen at the Schiff base is exchanged by deuterium
- E^{in}_{pr} energy density of incoming probe pulse
- E^{out}_{pr} energy density of outgoing probe pulse
- h Planck's constant
- I light intensity after absorbance
- I_o incident light intensity
- $\Delta I/I_o$ relative change of transmitted light intensity
- I_{ex} intensity of excitation pulse
- I_{pr} intensity of probing (interrogating) pulse
- J first ground-state intermediate in the photocycle of BR
- K second ground-state intermediate in the photocycle of BR
- $K(t)$ cross-correlation function between exciting and probing pulses
- ℓ path length of the sample
- L intermediate in the photocycle of BR
- M intermediate in the photocycle of BR
- N_i number densities of BR, S_1, J, and K (for i = BR, S_1, J, K)
- $\tilde{N}_i(t_D)$ calculated transmission change for the probe pulse induced by the state i (for i = BR, S_1, J, K)
- O intermediate in the photocycle of BR
- S_o ground state
- S_1 first excited state
- t time
- t_D delay time between the exciting and probing pulse
- t_p duration (FWHM) of picosecond light pulse
- T transmission
- T_c width (FWHM) of cross-correlation trace
- λ wavelength
- λ_{ex} excitation wavelength
- λ_{pr} probing (interrogating) wavelength
- η quantum yield of the photocycle in BR
- η_{fl} fluorescence quantum yield
- η_J efficiency for the formation of J
- σ_i absorption cross section (for i = BR, S_1, J, K)
- σ_{BR} absorption cross section of BR at the probing wavelength
- $\tilde{\sigma}_{BR}$ absorption cross section of BR at the excitation wavelength
- $\Delta_{\sigma J}$ $= \sigma_J - \sigma_{BR}$
- $\Delta_{\sigma K}$ $= \sigma_K - \sigma_{BR}$
- τ_{fl} lifetime of fluorescence
- τ_1 lifetime of S_1
- τ_1 rise time of J
- τ_2 decay time of J, rise time of K
- τ_{rad} radiation lifetime
- υ frequency of light pulse

MATERIAL PREPARATION

The purple membrane fragments were isolated from *Halobacterium halobium* strain S9 according to the method described in reference 21. The purified membranes were suspended in 0.01 M potassium phosphate buffer (pH 7) to an optical density of 8 at 570 nm.

The membrane fragments were measured in optical cells with a path length of 1 mm yielding an absorbance $A(570\text{ nm}) = -\ell g\, T/I_o = 0.8$. The experiments were carried out at room temperature (T = 23°C). All measurements were made with light-adapted samples prepared by standard illumination of the suspension (30 min, 150 W, $\lambda \geq 450$ nm). In picoseconds experiments, a light exposure of 3 s between two laser shots kept the sample in the light-adapted state. Before and after each picosecond experiment, the absorption spectrum of the sample was recorded. Spectral changes indicating denaturation of the BR suspension were not observed under our experimental conditions.

The deuterated samples were prepared by suspending the purified membrane fragments in D_2O. After illuminating the sample (1 h, 900 W Xe-lamp, $\lambda \geq 450$ nm) the membrane fragments were isolated by centrifugation and subsequently resuspended in D_2O. This treatment was repeated twice. The optical density at 570 nm was finally adjusted to 8.

EXPERIMENTAL

Several optical techniques were applied in our investigations. Time resolved absorption changes were measured with a set-up shown in Fig. 1. Single picosecond light pulses ($t\rho \simeq 4$ ps) were generated by a mode-locked Nd-glass laser system of low repetition rate (0.25 Hz). The single pulses were divided by a beam splitter BS into two parts. The excitation pulse (beam 1) was first frequency converted (FC-I in Fig. 1) to the second harmonic wavelength of 527 nm and then transformed by transient stimulated Raman scattering to 540 nm. The interrogating probing pulse (beam 2) was delayed by an optical delay line and frequency shifted by three different frequency converters depending on the specific experiments (FC-II in Fig. 1). (*a*) A combination of coherent and stimulated Raman scattering gave pulses with a superior time resolution of 0.3 ps (22). This method was used at the probing wavelengths λ_{pr} = 555 nm and λ_{pr} = 640 nm. (*b*) A traveling wave frequency converter (23) generated the probing pulses of $\lambda_{pr} > 555$ nm. (*c*) A picosecond light continuum was generated in beam 2, and various frequency components were selected by interference filters with a bandwidth of 10 nm.

The frequency shifted probing pulses were subdivided into two parts that both traveled through the sample. One pulse monitored excited molecules, while the other pulse served as a reference. The diameter of the exciting beam was larger than that of the probing beam to keep the excitation constant over the probed area. The two probing beams transmitted through the sample were imaged onto the photo-diodes of a difference detector. The difference detection system of high precision

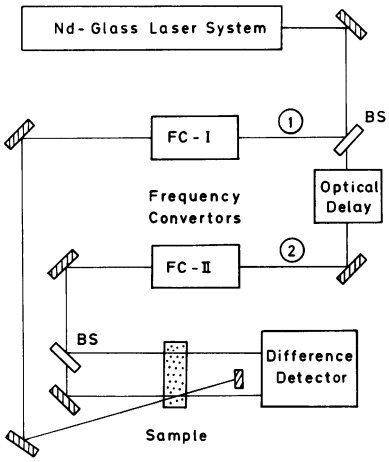

FIGURE 1 Scheme of the experimental set-up for the measurement of time-dependent absorption changes. Single picosecond light pulses from a mode-locked Nd-glass laser system are split into exciting (1) and probing (2) pulses by a first beam splitter BS. Both pulses are frequency tuned by different frequency converters, FC-I and FC-II. A difference detection system measures the transmission change of the probing pulse as a function of the time delay t_D between exciting and probing pulse. The exciting pulse (1) ends at a beam stop.

allowed to measure small transmission changes (24). Variations of the transmitted light energy induced by the exciting pulses of $\Delta I/I = 5 \times 10^{-4}$ could be measured. Changes of the sample transmission were recorded as a function of the time delay between the excitation and the probing process. The interrogating pulses (I_{pr}) were weaker than the exciting pulses (I_{ex}) by a factor of at least 20: $I_{ex}/I_{pr} \geq 20$. The probing pulses were polarized parallel to the exciting pulses.

Time resolution and time zero were deduced after each measurement from the cross-correlation trace between exciting and probing pulses measured in a nonlinear crystal. In the general practice of nonlinear optics, time resolution is understood as the shortest time constant of a dynamic process that can be measured with a given experimental system. Time resolution depends strongly on the experimental conditions such as: (*a*) Duration of the light pulses, (*b*) steepness of the wings of the light pulses, (*c*) temporal correlation between exciting and probing pulses, (*d*) precision of data acquisition and (*e*) signal-to-noise ratio. If the time constants to be measured are shorter than the halfwidth of the cross-correlation function, it is obvious that deconvolution procedures have to be used to deduce the molecular time constants. A demonstration of the time resolution of the experimental set-up used in our experiments is given in reference 22. These results demonstrate the capability of our equipment to measure time constants down to 0.3 ps. The experimental conditions of reference 22 were very similar to the conditions in the experiments reported here.

Time resolved fluorescence studies were made using the frequency doubled picosecond pulses of the Nd-glass laser system for excitation of the sample (λ_{ex} = 527 nm) and a streak camera to record the fluorescence emission. The time dependence of the fluorescence ($\lambda \geq 570$ nm) was corrected for nonlinearities of the camera.

The stationary fluorescence spectrum was measured with an argon ion laser (λ_{ex} = 514 nm) as excitation source at an intensity level in the sample of 10^{-3} W/cm^2. A monochromator/photomultiplier combination was used to record the spectrum with a spectral bandwidth of $\Delta\lambda$ = 3 nm. Fluorescence was corrected for reabsorption of the sample and for the spectral sensitivity of the detection system.

Special care had to be taken when the fluorescence of BR was measured. Since the fluorescence is very weak, several tests were performed to assure that the fluorescence of BR was indeed observed. Fluorescence from intermediates in the photocycle was excluded by measuring at low excitation levels (increasing the excitation by a factor of 10 did not change the fluorescence spectrum). Fluorescence from impurities could be ruled out by the following experiment. A membrane suspension in which BR was converted to the apoprotein bacterioopsin (25) was measured and no fluorescence emission of this sample was found. The fluorescence quantum yield η_{fl} was determined by comparing the BR fluorescence emission with that of the dye oxazine-1 in ethanol (η_{fl} = 0.11) (26).

RESULTS

Fluorescence Spectrum

Fig. 2 shows the absorption and the fluorescence spectrum of light-adapted BR, both being similar to previously published spectra (27). The absorption band is very broad and extends from the near ultraviolet (UV) to the maximum in the visible ~570 nm. The fluorescence band is also broad and featureless. It peaks ~730 nm and extends to the near infrared. The fluorescence of BR shows two interesting features: (*a*) The fluorescence emission is strongly red-shifted. A Stokes shift of ~4,800 cm^{-1} is found. (*b*) The fluorescence quantum yield η_{fl} is very low, $\eta_{fl} = (1 \pm 0.5) \times 10^{-4}$. This finding suggests that the fluorescing excited singlet state of BR has a very short lifetime. One estimates from the absorption band of BR a radiative lifetime of τ_{rad} = 7 ns (28), which leads to an excited singlet-state lifetime $\tau_1 \simeq \eta_{fl} \times \tau_{rad}$ = 0.7 ps.

Degree of Excitation

Most of the previous time resolved experiments of the primary steps of the photocycle of BR were carried out at high intensities. To show the influence of strong irradiation on the properties of BR, we measured the transmission of a BR sample with picosecond light pulses (t_p = 4 ps, λ = 527 nm) as a function of the light intensity. At low intensities the transmission is constant. For intensities above 10^9 W/cm^2 the transmission increases substantially, which results from the excitation of BR. Up to intensities of 1.5 ×

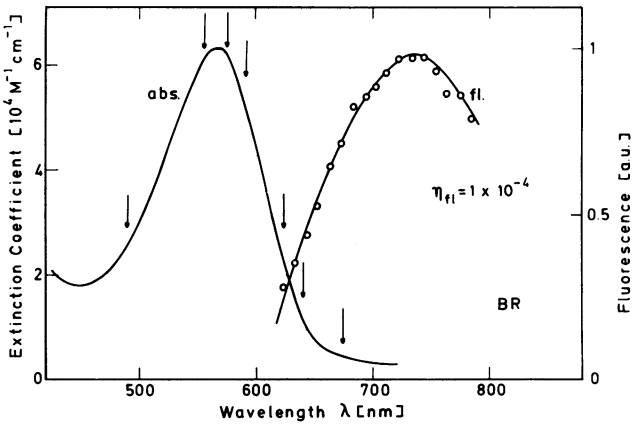

FIGURE 2 Absorption and fluorescence spectra of light-adapted bacteriorhodopsin. A fluorescence quantum yield of $\eta_{fl} = 1 \times 10^{-4}$ was measured. The various wavelengths of the probe pulses used in Figs. 4–6 are marked by arrows.

10^{10} W/cm^2 a reversible bleaching is observed, i.e., the transmission of the sample returns to its initial value within the pulse separation of 4 s. At higher intensities an irreversible destruction of the sample occurs.

For this reason, in our excite and probe experiments a weak excitation of I_o = 170 MW/cm^2 was used. At this intensity ~10% of the BR molecules absorb one photon per pulse. This light energy, when applied to the BR sample within 4 ps, approximately corresponds to the physiological condition of sun light falling onto the same sample within the turnover time of BR, i.e., 10 ms. In other words, the same number of BR molecules start a photocycle when excited with the laser beam as are cycling under constant illumination by sun light.

Transient Absorbance Changes of BR on the Picosecond Time Scale

Essential information on the dynamical properties of BR may be deduced from the time dependent absorbance change ΔA. The BR sample was excited at λ = 540 nm with single pulses of 3 ps duration. Probing pulses measured the transmission of the sample as a function of the time delay between excitation and probing at seven wavelengths (see arrows in Fig. 2). In Figs. 3, 4, 5, and 7 experimental data are shown as full or open circles. They represent mean values over 15 individual measurements; the curves in these figures are calculated using the model of Fig. 8.

Fig. 3 shows the experimental results for a probing wavelength of λ_{pr} = 555 nm, which is close to the peak of the BR absorption band. The absorbance change induced by the exciting pulse $\Delta A = A(t_D) - A(-\infty)$ is plotted vs. the delay time t_D. The absorbance decreases rapidly during the excitation indicating a depopulation of the ground state and the population of the excited singlet state S_1 of BR. The absorbance decrease reaches its maximum at t_D = 2 ps. At later delay times the absorbance recovers to some extent with a time constant of 5 ps. Delaying the probe pulse by >15 ps reveals a constant absorbance change ΔA, which remains during the total observation time of 300 ps (Fig. 3 *b*). From this measurement it becomes evident that after excitation of BR a long-lived photoproduct with reduced absorbance at λ_{pr} = 555 nm is built up with a time constant of 5 ps. We call this state *K*, and mention that this term was introduced by Lozier et al. on the basis of nanosecond experiments. The questions whether the species *K* we are observing in our picosecond experiments is identical to the species in the nanosecond range remains open.

More information on *K* is obtained from the measurements on the long-wavelength side of the BR band (see Fig. 4). A rapid increase of the absorbance is found during and after excitation. The rise of absorbance varies with the wavelength (see Fig. 4 *a–c*). Part of the absorbance increase relaxes with the same time constant of 5 ps as found at λ_{pr} = 555 nm. For later delay times, 15 ps > t_D > 300 ps, the enhanced absorbance persists. The curves of Fig. 4 indicate that the long-lived state *K* is formed with a

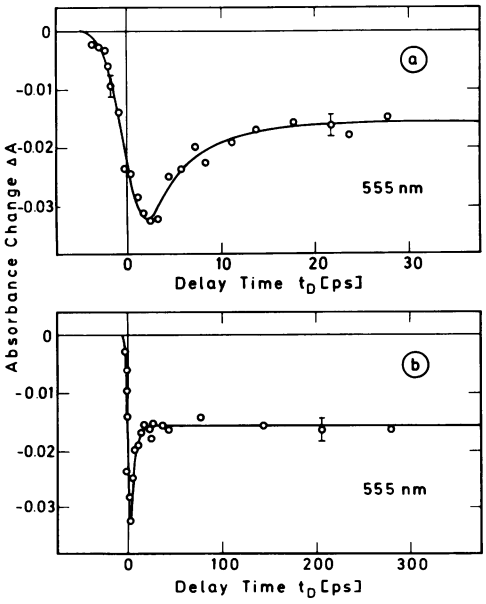

FIGURE 3 Absorbance changes induced by pulses at λ_{ex} = 540 nm and monitored by pulses at λ_{pr} = 555 nm. The rapid absorbance decreases ~t_D = 0 reflects the depopulation of the ground state S_o. At $t_D \geq 2$ ps the formation of the intermediate photoproduct *K* with a time constant of τ_2 = 5 ± 1 ps is observed (Fig. 3 *a*). After t_D > 15 ps the absorbance change remains constant for the experimental time of 300 ps (Fig. 3 *b*).

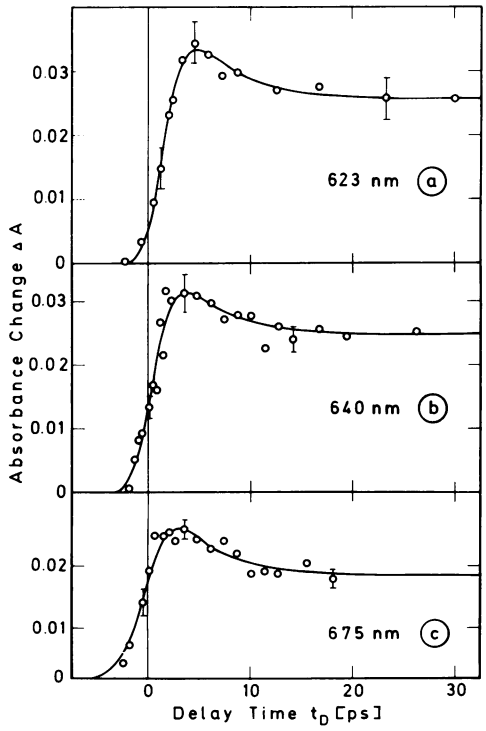

FIGURE 4 Time resolved transmission measurements after excitation with λ_{ex} = 540 nm. Probe pulses are at λ_{pr} = 623, 640, and 675 nm. Note that ~t_D = 5 ps the absorption of the photoproduct *K* appears.

time constant of 5 ps. The different shapes of the curves around time zero in Fig. 4 give a first indication that K is not formed directly from the excited singlet state S_1 of BR but is preceeded by a short-lived photoproduct, which we call J according to reference 29.

A clear demonstration of the excited singlet state S_1 of BR and of the intermediate J is obtained from the transient absorbance data shown in Fig. 5. The absorbance changes at λ_{pr} = 492, 575, and 592 nm exhibit a rather complicated time dependence. Rapid absorbance changes occur, peaking close to $t_D = 0$. The transient bleaching at 575 and 592 nm and the transient increase of absorption at 492 nm decay with time constants shorter than 2 ps. At later times the long-lived absorbance change due to K (see Fig. 3 *b*) is found.

The rapid absorbance change around time zero is related to the excited state of BR populated during the optical excitation. The increased absorption around 492 nm indicates that the excited state has an absorption cross section $\sigma_{BR_{S1}}$ larger than the absorption cross section of σ_{BR} at 492 nm. AT λ_{pr} = 575 and 592 nm, however, the cross sections of the ground state are larger than that of the excited state (see Fig. 10). From the excited singlet state S_1 the intermediate J is formed. The change of the signal curves in Fig. 5 around t_D ~2 ps indicates that J is formed with a time constant $\tau_1 < 1$ ps.

The experimental data presented up to now indicate that the system passes through at least three different states within the first picoseconds. The excited singlet state S_1 of BR is populated first; it has a lifetime of $\tau_1 < 1$ ps. Within 1 ps an intermediate, J, is formed that decays with a time constant of 5 ps into the long-lived photoproduct K.

Transient Difference Spectra

The spectroscopic properties of the intermediates J and K may be deduced from the absorbance change measured as a function of wavelength at certain fixed delay times. In Fig. 6 the full circles represent the difference spectrum of BR and K taken at t_D = 100 ps. At this late time the difference spectrum is solely related to the state K. In the spectral range of the BR absorption band around λ = 570 nm the absorbance decreases, i.e., BR molecules are transformed to the intermediates K. The higher absorbance ~610 nm indicates that the absorption of the state K is red-shifted, relative to the absorption of light-adapted BR. The difference spectrum taken at t_D = 5 ps (open circles in Fig. 6) reflects contributions from both, K and J. Comparison with the data at t_D = 100 ps gives information on the spectral properties of the intermediate J. J has an absorption spectrum similar to that of K, but is more red-shifted. For a quantitative determination of the absorption spectra J and K, the excitation density and the relative efficiency η_J for the formation of the intermediates J and K after excitation of BR must be known. They are presented in the Discussion below.

We also measured the absorbance increase ΔA of K (λ = 670 nm, t_D = 100 ps) as a function of the angle between the

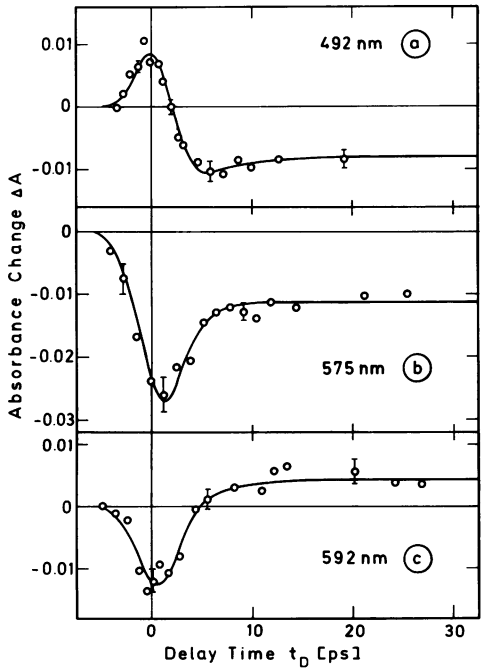

FIGURE 5 Time resolved absorption measurements for probing wavelengths λ_{pr} = 492, 575, and 592 nm. The fast absorbance changes are caused by the excited singlet state S_1 of BR. At λ_{pr} = 492 nm excess absorbance, i.e., excited-state absorption is observed. The calculated curves suggest an excited-state lifetime of ~0.7 ps.

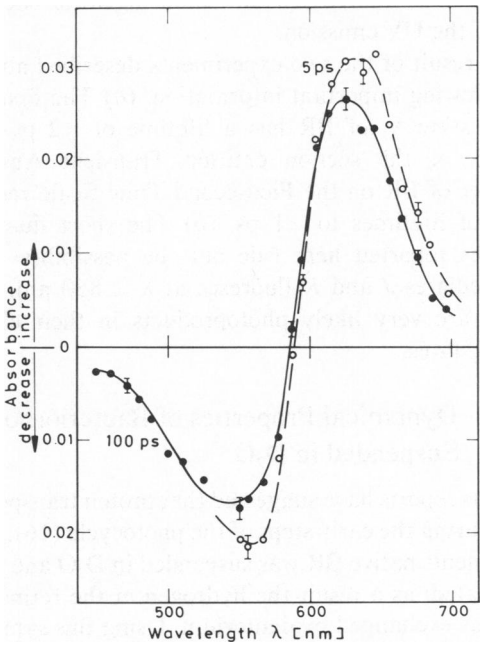

FIGURE 6 Difference spectra of light-adapted bacteriorhodopsin measured at delay times t_D = 5 ps (circles, dashed line) and t_D = 100 ps (full points, solid line) after excitation at λ_{ex} = 540 nm. The curve at 5 ps provides information on both intermediates J and K, whereas the curve at t_D = 100 ps solely reflects the absorption properties of K.

polarization of the exciting and probing pulses. The dichroitic ratio was found to be $\Delta A_{\parallel}/\Delta A_{\perp} = 2.6 \pm 0.5$. Its significance for the direction of the transition moment of BR and *K* are discussed later.

Evidence for the Short Lifetime of the Excited Singlet State

More information on the population and the lifetime of the excited singlet state of BR after absorption of light is obtained by the following two experiments: (*a*) The fluorescence emission ($\lambda_{fl} \geq 570$ nm) was measured with a streak camera after excitation with pulses of 4 ps duration. The fluorescence trace was found to follow the time evolution of the exciting laser pulse. Taking into account the time resolution of the streak camera one deduces a lifetime of the fluorescence state of $\tau \leq 2$ ps. (*b*) UV emission ~300 nm was found in BR after two-step excitation in the visible. From the first excited singlet state S_1 generated by a first pulse P1 absorption of light from a second pulse P2 leads to higher singlet states from which the UV emission results. One can deduce the lifetime of the first excited singlet state by recording the yield of the UV emission as a function of the time delay between P1 and P2. Experimentally, we used pulses of 3 ps duration and at $\lambda_1 = 540$ nm and $\lambda_2 = 620$ nm. The fluorescence yield at 300 nm $\leq \lambda_{fl} \leq$ 400 nm was measured. The observed curve followed within the experimental accuracy the cross-correlation trace between the two pulses P1 and P2. This result provides the second argument that the intermediate state S_1 has a lifetime shorter than $\tau \leq 2$ ps. This time resolution is limited by the small signal-to-background ratio of the UV emission.

The result of the two experiments described above give the following important information: (*a*) The first excited singlet state S_1 of BR has a lifetime of <2 ps and the findings of the section entitled Transient Absorbance Changes of BR on the Picosecond Time Scale reduce the range of lifetimes to <1 ps. (*b*) The short fluorescence lifetimes reported here rule out the possibility that the intermediates *J* and *K* fluoresce at $\lambda < 850$ nm. Thus, *J* and *K* are very likely photoproducts in their electronic ground states.

Dynamical Properties of Bacteriorhodopsin Suspended in D_2O

Previous reports have suggested that proton transport takes place during the early steps of the photocycle (16). In these experiments native BR was suspended in D_2O and strongly illuminated; as a result the hydrogen at the retinal Schiff base was exchanged by deuterium. Using this same procedure we prepared samples for the study of time resolved absorbance changes in deuterated BR. The exchange of the hydrogen at the Schiff base was controlled by resonance Raman scattering (pumping source Ar^+-ion laser, $\lambda = 514$ nm, intensity $I = 0.1$ W/cm^2). Peaks at 1,621 cm^{-1} (BR in D_2O) and at 1,642 cm^{-1} (BR in H_2O) were found. They have been assigned to the *C*=*N* stretching vibration of the deuterated and protonated retinal Schiff base, respectively (30–32). Our deuterated sample exhibits only the band at 1,621 cm^{-1}. From these data it can be estimated that at least 90% of the Schiff base hydrogens are replaced by deuterium.

The measurements of the transient absorbance changes described in the Transient Absorbance Changes of BR on the Picosecond Time Scale section were repeated with the deuterated samples, but no indication of a deuterium effect was found. The transient absorbance curves of deuterated and native BR are identical. As an example, the results at three probing wavelengths $\lambda_{pr} = 492$, 575, and 675 nm are depicted in Fig. 7. The measured absorbance changes of d-BR (full points) should be compared with those of native BR (open circles).

We conclude from these results that the first events in the photocycle are not affected by deuteration, because the relevant time constants that are the lifetime of the S_1 state and the build-up time of *K* differ in the deuterated and native BR samples only within the experimental error of 20%.

DISCUSSION

In this section we present a model for the first events of the photocycle of BR that accounts quantitatively for the

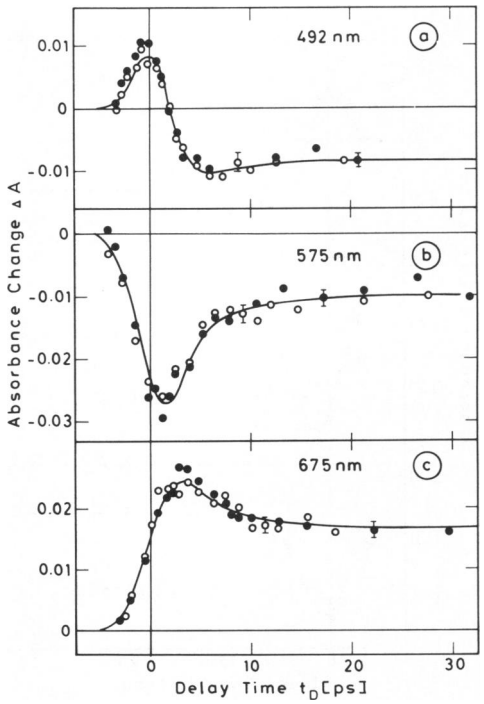

FIGURE 7 Absorbance changes of probing pulses at $\lambda_{pr} = 492$, 575, and 675 nm using deuterated BR samples (full points) and native bacteriorhodopsin (open circles). Excitation wavelength was $\lambda_{ex} = 540$ nm. Within the experimental error the same transient absorption changes for BR in H_2O and BR in D_2O were observed.

experimental data presented above. The dynamics of the model are described by rate equations. Quantitative information of the absorption spectra of the first excited singlet state of BR and of the intermediates J and K are elicited by fitting calculated curves to the data points of Figs. 3–5. Next, the influence of the trimeric nature of BR on its photophysics is discussed. Finally, the observed intermediates are related to molecular processes of retinal in the protein matrix.

Model of the Early Events of Bacteriorhodopsin

In the previous sections we presented a series of observations that point to very rapid processes during and immediately following optical excitation of BR. The most simple model that is compatible with out results is schematically depicted in Fig. 8. The mathematical treatment of the model is given below.

Light-adapted BR of number density N_{BR} is first optically excited to a vibronic level of the first excited singlet state BR_{S1}. We designate the absorption cross section of BR at the excitation and probing wavelength with $\tilde{\sigma}_{BR}$ and σ_{BR}, respectively. The lifetime τ_1 of the excited state BR_{S1} is very short (<1 ps). Several observables originate from BR_{S1}: the short visible fluorescence, the excited-state absorption with cross section $\sigma_{BR_{S1}}$ (which leads to UV fluorescence) and the formation of the first photoproduct J with an efficiency of formation η_J. The second photoproduct K is subsequently formed with a time constant τ_2; it is stable at least for the time of our observation of 300 ps. The exciting pulse has a low intensity $I_{ex}(t)$ at frequency ν. Thus, only small values of N_{S1} ($N_{S1} << N_{BR}$ occur. The two-step absorption to higher singlet states does not change N_{S1} significantly and may be neglected for the calculation of N_{S1}; but $\sigma_{BR_{S1}}$ has to be considered when the transmission of the probing pulses is calculated. The time dependence of the number density of the four states BR, S_1, J, and K is governed by the following rate equations:

$$\frac{\partial N_{BR}}{\partial t} = -\frac{\tilde{\sigma}_{BR}}{h\nu} I_{ex}(t) N_{BR} + \frac{(1-\eta_J)}{\tau_1} N_{s1} \quad (1)$$

$$\frac{\partial N_{s1}}{\partial t} = \frac{\tilde{\sigma}_{BR}}{h\nu} I_{ex}(t) N_{BR} - \frac{1}{\tau_1} N_{s1} \quad (2)$$

$$\frac{\partial N_J}{\partial t} = \frac{\eta_J}{\tau_1} N_{s1} - \frac{1}{\tau_2} N_J \quad (3)$$

$$\frac{\partial N_K}{\partial t} = \frac{1}{\tau_2} N_J \quad (4)$$

Experimentally, we determine the momentary number densities N_i by the energy transmission T of the probe pulses I_{pr} of finite pulse duration.

$$T = \int_{-\infty}^{\infty} I_{pr}^{out}(t)dt \Big/ \int_{-\infty}^{+\infty} I_{pr}^{in}(t)dt = E_{pr}^{out}/E_{pr}^{in},$$

i.e., the transmission is the ratio of the time averaged intensities (I_{out}, I_{in}). The observed signal $\tilde{N}_i$ corresponds to the convolution of N_i with I_{pr}:

$$\tilde{N}_i(t_D) = \frac{1}{E_{pr}^{in}} \int_{-\infty}^{+\infty} N_i(t)\, I_{pr}^{out}(t - t_D)dt$$

$$\text{for } i = BR, S_1, J, K, \quad (5)$$

where E_{pr}^{in} denotes the energy density of the incoming probe pulse (the time integral over the probe pulse intensity). In our investigations we measured weak absorption changes ΔA for various delay times at various wavelengths of the probing pulses (λ_{pr}). In the general case, four species contribute to the absorption changes ΔA at any wavelength λ_{pr}: BR, its excited singlet state BR_{S1} and the photoproducts J and K.

$$\Delta A(t_D) = \{\sigma_{BR}[\tilde{N}_{BR}(t_D) - \tilde{N}_{BR}(-\infty)] + \sigma_{BR_{s1}}\tilde{N}_{s1}(t_D) + \sigma_J\tilde{N}_J(t_D) + \sigma_K\tilde{N}_K(t_D)\}\ell, \quad (6)$$

where ℓ is the optical path length of the sample. The cross sections σ_i (i = BR, S_1, J, K) are strongly wavelength dependent. The set of Eqs. 1–6 may be simplified by two approximations that are well justified for the weak excitation in our experiments. (*a*) Small changes in the ground-state population, i.e., $|N_{BR}(t_D) - N_{BR}(-\infty)| << N_{BR}(-\infty)$ are produced and (*b*) conservation of number densities $N_{BR}(-\infty) = N_{BR}(t) + N_{S1}(t) + N_J(t) + N_K(t)$ is guaranteed. Under these conditions the four differential Eqs. 1–4 are reduced to three. With an appropriate transformation it is possible to rewrite Eq. 6 in the form

$$\Delta A(t_D) = \sum_{j=1}^{3} a_j M_j(t_D)\ell \quad (7)$$

with the parameters

$$a_1 = \sigma_{BR_{s1}} - \sigma_{BR} - \frac{\tau_2\eta_J}{\tau_1 - \eta_1}(\sigma_J - \sigma_{BR}) + \frac{\tau_1\eta_J}{\tau_2 - \tau_1}(\sigma_K - \sigma_{BR}) \quad (8)$$

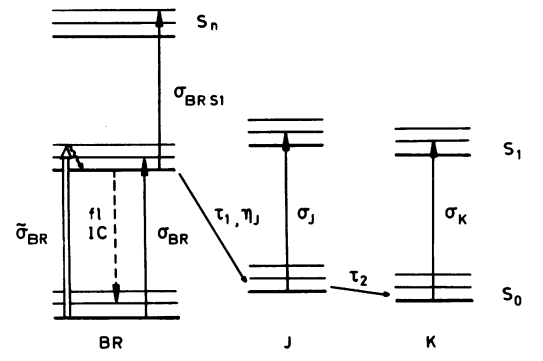

FIGURE 8 Level scheme for the first intermediates describing the transient properties of bacteriorhodopsin on the picosecond time scale. Important species are BR ground state, BR excited singlet state (BR_{S1}), ground-state intermediate J, ground-state intermediate K, with their corresponding absorption cross sections σ_{BR}, $\sigma_{BR_{S1}}$, σ_J, σ_K. The relaxation time of BR_{S1} is τ_1, that of state J is τ_2.

$$a_2 = \frac{\tau_2 \eta_J}{\tau_2 - \tau_1} (\sigma_J - \sigma_K) \quad (9)$$

$$a_3 = \eta_J (\sigma_K - \sigma_{BR}) \quad (10)$$

and with

$$M_j(t_D) = \frac{\tilde{\sigma}_{BR} N_{BR}(-\infty)}{h\nu} \int_{-\infty}^{t_D} dt\, K(t) \exp\left(\frac{t - t_D}{\tau_j}\right), \quad \text{for } j = 1, 2, 3 \quad (11)$$

where $K(t)$ stands for the cross-correlation function between exciting and probing pulses. The maximal number of 3 for j reflects the minimal number of differential equations necessary for the description of the model. The relaxation times τ_1, τ_2, and τ_3 are those of BR_{S1}, J, and K. The transformation made here has the advantage that Eq. 7 together with Eqs. 8–11 are very convenient to describe the experimental data. The functions M_j are readily evaluated. They contain, besides the measured cross-correlation function $K(t)$, the time constants τ_i, which could be directly deduced from Figs. 3–5.

The a's in Eq. 7 are obtained by adapting the calculated curves to the experimental data points in Figs. 3–5. The evaluation of the experimental data yielded $\tau_1 < 1$ ps, $\tau_2 = 5$ ps, and $\tau_3 >> 300$ ps (i.e., $\tau_3 >> \tau_1, \tau_2$). The solid lines in Figs. 4–6 represent the best fit using Eqs. 7–11, where $\tau_1 = 0.7$ ps, $\tau_2 = 5$ ps, and $\tau_3 = \infty$. To test the precision of the time constants we changed τ_1 from 0.7 to 1.2 ps. This resulted in a considerable decrease of the quality of the fit measured as an increase of the mean deviation by a factor of 20. With the help of the a's the absorption cross sections σ_i of the three states BR_{S1}, J, and K are determined. Repeating this procedure at the various wavelengths, the absorption spectrum of BR_{S1} is deduced. Spectra of photoproducts J and K are obtained from the measured difference spectra of Fig. 6 by using the above mentioned time constants $\tau_1 - \tau_3$ and the quantum efficiency η_J.

In the rate equations and in the equations of the coefficients a_i (Eqs. 8–10) the efficiency η_J for the formation of the state J enters. Unfortunately, there exists considerable uncertainty in the literature on the efficiency η of the photocycle of BR. Some papers report values of $\eta = 0.3$ (33–37), whereas higher efficiencies of $\eta = 0.6$ have been found by other authors (38). On account of this uncertainty we made the calculations for the absorption spectra for the two values of η_j.

The absorption spectra of the two intermediates J and K are depicted in Fig. 9 together with the absorption band of BR. The spectra are obtained applying Eq. 7 to the experimental data of Figs. 3–6. Different band shapes are found when the values of $\eta_J = 0.3$ and $\eta_J = 0.6$ are used for the calculated spectra of Figs. 9 a and b, respectively. For both values of η_J the absorption spectra of the intermediates J and K are red-shifted relative to BR. The bands of K peak at 605 or 590 nm for $\eta_j = 0.3$ or $\eta_J = 0.6$,

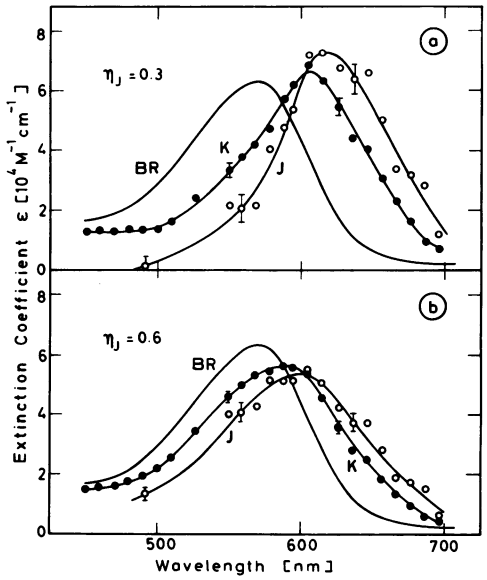

FIGURE 9 Absorption spectra of bacteriorhodopsin and of the photoproducts J and K. The spectra are calculated using the model of Fig. 8 and the transient absorption spectra of Fig. 6. A primary quantum yield for the formation of J of $\eta_J = 0.3$ and $\eta_J = 0.6$ was assumed for the calculation of the spectra in Fig. 9 a and b, respectively.

respectively. J-bands have their maxima at the wavelengths 615 ($\eta_J = 0.3$) and 600 nm ($\eta_J = 0.6$).

We favor the results obtained with $\eta_J = 0.6$ for three reasons: (a) New experiments, where the formation of the intermediate M was carefully investigated, suggest $\eta_J = 0.6$ (39). (b) The extinction coefficient of the J intermediate comes out to be unreasonably small at short wavelengths, if $\eta_J = 0.3$ is assumed (see Fig. 9 a). (c) The intermediate K on the picosecond time scale is likely to be identical with the previously described K state on the nanosecond time scale; i.e., the peak of the K band at 590 nm in Fig. 9 b ($\eta_J = 0.6$) agrees well with the K intermediate on the nanosecond time scale (4).

We now turn to the discussion of the absorption cross-section of the first excited singlet state $\sigma_{BR_{S1}}$. As pointed out above, a significant excited-state absorption occurs only at very early times (at t_D around zero). The analysis for $\sigma_{BR_{S1}}$ is simplified, since in this early time domain the formation of the K intermediate is negligible, i.e., $N_K = 0$. Inspection of Eqs. 7–12 shows that $\sigma_{BR_{S1}} = \sigma_{BR} + a_1 + a_2 + a_3$ is independent of η_J.

In Fig. 10 the cross section of the excited state $\sigma_{BR_{S1}}$ is plotted vs. wavelength. The data are deduced from the absorption changes documented in Figs 3–5. The absorption band of the ground state S_0 of BR is redrawn in Fig. 10 for convenient comparison of the ground and the excited state, σ_{BR}, and $\sigma_{BR_{S1}}$, respectively. According to the data of Fig. 10 the values of $\sigma_{BR_{S1}}$ are strongly dependent on the wavelength. At short wavelengths the excited-state absorption even exceeds the absorption from the ground state.

Our experimental data using the model of Fig. 8 (i.e., with the Eqs. 7–11) allow us to estimate a lower limit for

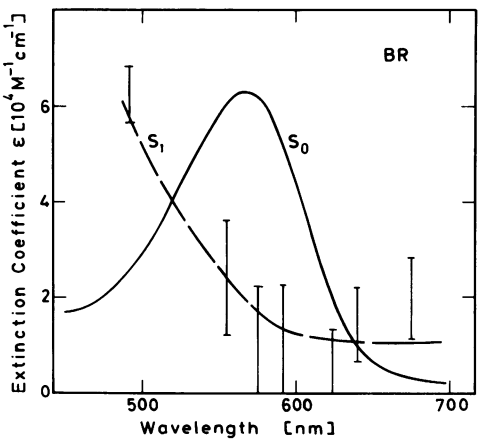

FIGURE 10 Absorption spectrum of the ground state of BR and of the first excited singlet state BR_{S1} (broken line). Strong excited-state absorption occurs at the short wavelength side. The bars indicate the precision of the spectra taking into account experimental uncertainties.

the lifetime of the excited singlet state, τ_1. One learns from Fig. 6 that $\Delta\sigma_J = (\sigma_J - \sigma_{BR})$ and $\Delta\sigma_K = (\sigma_K - \sigma_{BR})$ are close to zero at the crossing wavelength of 592 nm. For this wavelength and for a half-width T_c of the cross correlation, $T_c >> \tau_1$, $T_c = 4.5$ ps, Eqs. 7–11 simply to give

$$\Delta A_{592}(t_D = 0) = \gamma(\sigma_{BR_{S1}} - \sigma_{BR})\tau_1/T_c \qquad (12)$$

$\gamma = 5.9 \times 10^{14}$ cm^{-1} is a parameter containing various quantities that were determined experimentally. Taking the experimental value of $\Delta A(t_D = 0)$ from Fig. 5 *c* and considering $\sigma_{BR_{S1}} = 0$ (at 592 nm) one estimates the lower limit of the relaxation time τ_1 to be $\tau_1 = 0.4$ ps.

Summarizing this section one may state: the experimental data of Figs. 3–6 are fully consistent with the model of Fig. 8 as demonstrated by the fact that the data points match the calculated curves. Furthermore, the absorption spectra of the short-lived excited singlet state BR_{S1} and of the two photoproducts *J* and *K* can be predicted. The data suggest a lower limit for lifetime of the excited state of $\tau_1 = 0.4$ ps. In our experiments we worked with pulses of 3 ps duration. The time resolution is ~0.3 ps, which determined the accuracy of the value of τ_1. The present data suggest $\tau_1 = 0.7 \pm 0.3$ ps. Experiments with a time resolution of 0.05 ps are now in progress. They yielded τ_1 values of 430 ± 50 fs (52), which is the lower limit of the range given above.

Trimeric Structure of Bacteriorhodopsin

Up to now we have considered BR as individual protein units. However, in the purple membranes investigated here three BR molecules are arranged around a threefold axis to form a trimer, which in turn builds up a hexagonal two-dimensional lattice (1). The absorption bands of the trimers and monomers are similar (40). Evidence for the existence of trimers comes from the circular dichroism. These measurements support an excitonic coupling within the trimer with a binding energy of ~200 cm^{-1} (41, 42). The coupling leads to a delocalization of the excitation energy over the three BR molecules of the trimer. After absorption of light by the trimer the excitation is delocalized for a very short time and quickly trapped into the excited S_1 state of one BR molecule. From this state the photoproducts *J* and subsequently *K* are produced.

The delocalization of the excitation energy in the trimer influences the dichroitic ratio $\Delta A_\parallel/\Delta A_\perp$ for the intermediate *K*. Detailed considerations show that the dichroitic ratio of the product state depends on the arrangement of the BR molecules in the trimer, the excitation wavelength, the angle between the transition moments of the BR monomer and the intermediate *K*, and rotational motions. An arrangement of all three transitions moments of the trimer within one and the same plane leads to $\Delta A_\parallel/\Delta A_\perp = 3$. A smaller dichroitic ratio, e.g., the measured value of 2.6 ± 0.5, may be obtained when the transition moments are not co-planar or when an angle exists between the transition moments of the monomeric BR and of the product state *K*. Rotational motion of the purple membrane fragments can be excluded on our time scale of 100 ps.

A Molecular Model of the Primary Events

Three molecular processes could occur in the picosecond time range after light absorption: (*a*) changes in the retinal configuration/conformation, (*b*) changes in the protein conformation, and (*c*) changes in protonation states. The latter process can be disregarded on the basis of our results that no deuterium effect was observed. This clearly indicates that proton movements to and from the retinal Schiff base are not involved in events occurring during the first few picoseconds, but are only of importance for later steps in the photocycle.

The scheme of the primary processes in BR (Fig. 11) is derived from our measurements and calculations fitting the experimental data and serves as a model for the interpretation of the molecular events accompanying the spectroscopic changes. Parts of the energy surfaces are shown schematically vs. a reaction coordinate that connects the BR trimer, the excited BR monomer, and the

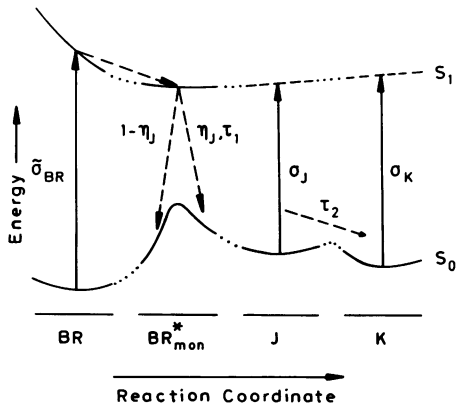

FIGURE 11 Scheme of the energy surfaces of bacteriorhodopsin vs. the reaction coordinate.

photoproducts J and K. Several important transitions are indicated by arrows. The model presented here agrees with the one published in reference 29, with respect to the fact that J is the first ground state intermediate.

The incident light is first absorbed by the BR trimers and trapped very rapidly in the excited state of one monomer subunit, BR^*_{mon}. The excited state is located at lower energy than the primary excited levels, as evidenced by the large Stokes shift of the fluorescence spectrum. The lifetime of BR^*_{mon} is very short, ~0.7 ps (430 ± 50 fs) (52). The excited retinal then returns either to the original ground state or to J with a probability η_J. MNDO calculations have shown that two reaction channels are open from the excited state to the ground state of the intermediate J (43, 44). Scheme I, a *trans* to 13-*cis* isomerization, Scheme II a *trans* to 13-*cis*, 14s-*cis* isomerization. The *trans* to 13-*cis* isomerization has been demonstrated experimentally in three independent experiments. First, configurationally blocked retinal analog structures such as Scheme I and Scheme II

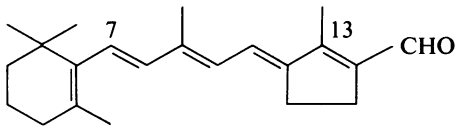

(*a*)

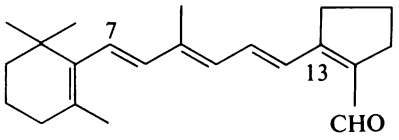

(*b*)

are able to reconstitute analog bacteriorhodopsins when mixed with bacterioopsin, but are photochemically and catalytically inactive (45). Second, a conformationally blocked retinal analog structure (Scheme III).

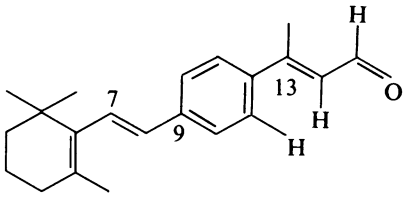

which is unable to adopt a planar 13-*cis* configuration, only reconstitutes a bacteriorhodopsin analog with its all-*trans* isomer, which is a protonated Schiff base (46). When this bacteriorhodopsin analog absorbs light, an excited state is reached, which has a lifetime of 10 ps and a 12-fold enhanced fluorescence quantum yield compared with BR (9). No photochemical product could be found and as a conclusion it was postulated that the primary photochemical reaction involves rotations around the C_{13} bond. Third, product K was shown by resonance Raman spectroscopy to be very likely a 13-*cis* configuration of retinal, possibly in a slightly distorted form (7). Whether the primary reaction to product J involves a concomitant rotation around the C_{14} bond, can so far only be postulated on the basis of two arguments. The concomitant rotation around the 13–14 and the 14–15 bond causes less motion of the molecular frame work in retinal, and less disturbance of the protein cavity (44) than a 13–14 bond rotation alone. Fig. 12 shows this two-bond rotation. In all four states (*a–d*) the retinal moiety is fixed to a rigid polypeptide backbone via the lysine 216 oligomethylene chain and the backbone is not allowed to change its position in any of its parts. State *a* is the ground state geometry, in *b* the carbon atom 14 has reached a position that roughly corresponds to an sp_3 hybridization state and to the energy minimum of the excited state in Fig. 11. From this state rehybridization either leads back to the original ground state with the probability $1 - \eta_J$ or the rotations are brought to completeness with η_J (Fig. 12 *c*). The change of the configuration of the retinal has profound consequences by changes in the sterical and electronic interaction of retinal and the protein. The distance of the positively charged nitrogen and its counterions presumably increases (seen by the red-shifted absorption maximum of J) and the retinal moiety exerts a strong pull on the polypeptide chain via the lysine methylene groups. It is interesting to note that the rotation of some of these methylene groups in the molecular model relaxes somewhat the steric strain (Fig. 12 *d*), which might be reflected by the transition from J to K.

Another explanation for the spectral changes assigned to the transition from state J into state K would be the following: Upon transition from the excited electronic state to the ground state a considerable amount of energy is lost in the retinal that heats the molecule. The increased temperature may cause changes in the absorption spectrum that decays with the cooling of the molecules. Experimentally, such processes are found to occur on the picosecond time scale (47). When this interpretation holds, the intermediates J and K differ only by the temperature of the chromophore in the sample.

With the transition into the ground state intermediates energy is stored via the change in the electronic and steric interactions compared to BR prior to excitation. This energy amounts to ~15 kcal/mol (48) and is used to drive the photocycle to completion as well as to deliver part of this energy to the proton to be translocated during the catalytic cycle. The fact that this energy of 15 kcal/mol has to be compared with 11.5 kcal/mol for a rotation around the 13–14 double bond (49) provides the second argument for a concomitant 13–14, 14–15 bond rotation upon excitation. This reaction would only be thermoreversible at the expense of 42 kcal and, therefore, be a configuration that allows the storage of the 15 kcal/mol observed experimentally (49).

Recently, resonance Raman spectra of BR and K were obtained that aimed for the identification of single-bond

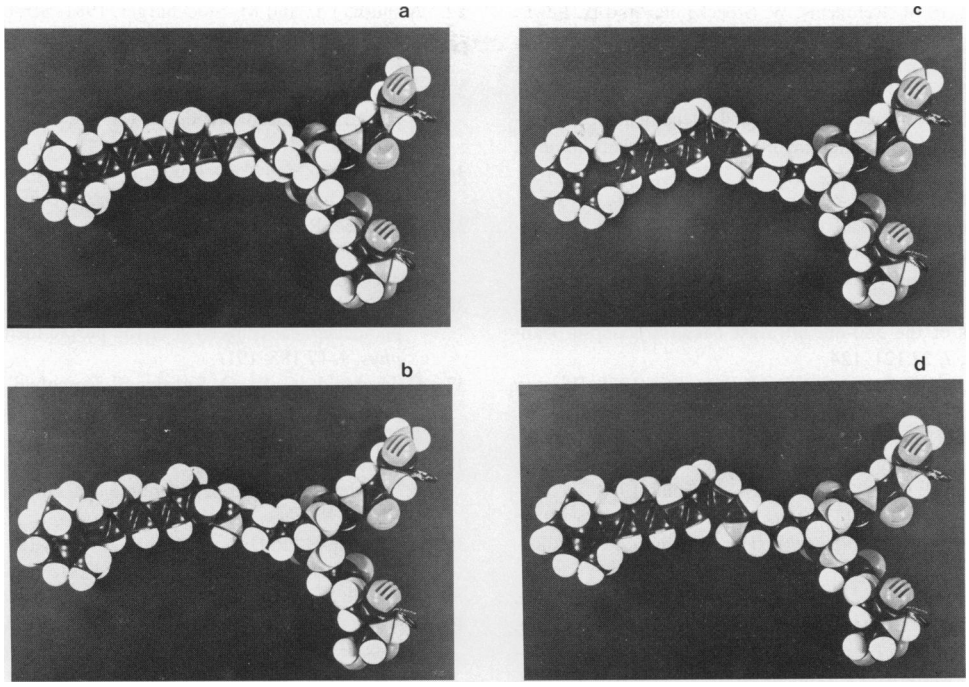

FIGURE 12 Molecular interpretation of the primary events in BR with a space-filling atomic model (according to [44]) (*a*) ground state; (*b*) excited state (S_1) with carbon 14 rotated by 90°; (*c*) primary photoproduct *J*; (*d*) relaxation of the oligomethylene chain of lysine 216 leading to intermediate *K*.

stretching modes. Interpretations of these spectra based on model calculations claimed that no 14 s-*cis* bond rotation is involved in *K*-formation (50). Improved model calculations based on the complete retinal molecule, however, are consistent with a 14 s-*cis* rotation (51). Only further experimental and theoretical investigations will finally answer this important question.

In conclusion, the data presented here allow a consistent description of the primary events of the photocycle of bacteriorhodopsin: absorption of a photon promotes bacteriorhodopsin onto the potential surface of the first excited electronic state. Here, the state BR_{S1} is reached. The rapid transition into the first ground-state intermediate occurs with 0.7 ± 3 ps (430 ± 50 fs) (52). A slower secondary process leads with 5 ps to the intermediate *K* stable for the first nanosecond. Several features of this picture agree with published values while others do not.

Note added in proof: While this manuscript was in press two papers appeared confirming our results. Sharkov et al. (1985. *Biochim. Biophys. Acta.* 808:94–102.) also investigated the primary events and published a rise time for *J* of 0.7 ps. Femtosecond experiments of our groups yielded a rise time for *J* of 430 ± 50 fs.

Received for publication 27 March 1985 and in final form 16 October 1985.

REFERENCES

1. Lanyi, J. K. 1984. Bacteriorhodopsin and related light-energy converters. *In* New Comprehensive Biochemistry. L. Ernster, editor. Elsevier/North Holland, Amsterdam. 315–350.
2. Smith, S. O., A. B. Myers, J. A. Pardoen, C. Winkel, P. P. J. Mulder, J. Lugtenburg, and R. Mathies. 1984. Determination of retinal Schiff base configuration in bacteriorhodopsin. *Proc. Natl. Acad. Sci. USA.* 81:2055–2059.
3. Harbison, G. S., S. O. Smith, J. A. Pardoen, C. Winkel, J. Lugtenburg, J. Herzfeld, R. Mathies, and R. G. Griffin. 1984. Dark-adapted bacteriorhodopsin contains 13-*cis*, 15-syn and all-*trans*, 15-anti retinal Schiff bases. *Proc. Natl. Acad. Sci. USA.* 81:1706–1709.
4. Lozier, R. H., R. A. Bogomolni, and W. Stoeckenius. 1975. Bacteriorhodopsin: a light-driven proton pump in *Halobacterium halobium*. *Biophys. J.* 15:955–962.
5. Kung, M. C., D. Devault, B. Hess, and D. Oesterhelt. 1975. Photolysis of bacterial rhodopsin. *Biophys. J.* 15:907–911.
6. Hsieh, C.-L., M. Nagumo, M. Nicol, and M. A. El-Sayed. 1981. Picosecond and nanosecond resonance Raman studies of bacteriorhodopsin. Do configurational changes of retinal occur in picoseconds? *J. Phys. Chem.* 85:2714–2717.
7. Braiman, M., and R. Mathies. 1982. Resonance Raman spectra of bacteriorhodopsin's primary photoproduct: evidence for a distorted 13-*cis* retinal chromophore. *Proc. Natl. Acad. Sci. USA.* 79:403–407.
8. Siebert, F., and W. Mäntele. 1983. Investigation of the primary photochemistry of bacteriorhodopsin by low temperature Fourier-transform infrared spectroscopy. *Eur. J. Biochem.* 130:565–573.
9. Polland, H.-J., M. A. Franz, W. Zinth, W. Kaiser, E. Kölling, and D. Oesterhelt. 1984. Optical picosecond studies of bacteriorhodopsin containing a sterically fixed retinal. *Biochim. Biophys. Acta.* 767:635–639.
10. Terner, J., C.-L. Hsieh, A. R. Burns, and M. A. El-Sayed. 1979. Time resolved resonance Raman spectroscopy of intermediates of bacteriorhodopsin: the bK_{590} intermediate. *Proc. Natl. Acad. Sci. USA.* 76:3046–3050.
11. Marcus, M. A., and A. Lewis. 1977. Kinetic resonance Raman spectroscopy: dynamics of deprotonation of the Schiff base of bacteriorhodopsin. *Science (Wash. DC).* 195:1328–1330.

12. Kaufmann, K. J., r. M. Rentzepis, W. Stoeckenius, and A. Lewis. 1976. Primary photochemical processes in bacteriorhodopsin. *Biochem. Biophys. Res. Commun.* 68:1109–1115.
13. Hirsch, M. D., M. A. Marcus, A. Lewis, H. Mahr, and N. Frigo. 1976. A method for measuring picosecond phenomena in photolabile species. The emission lifetime of bacteriorhodopsin. *Biophys. J.* 16:1399–1409.
14. Alfano, R. R., W. Yu, R. Govindjee, B. Becher, and T. G. Ebrey. 1976. Picosecond kinetics of the fluorescence from the chromophore of the purple membrane protein of *Halobacterium halobium. Biophys. J.* 16:541–545.
15. Kaufmann, K. J., V. Sundström, T. Yamane, and P. M. Rentzepis. 1978. Kinetics of the 580-nm ultrafast bacteriorhodopsin transient. *Biophys. J.* 22:121–124.
16. Applebury, M. L., K. S. Peters, and P. M. Rentzepis. 1978. Primary intermediates in the photochemical cycle of bacteriorhodopsin. *Biophys. J.* 23:375–382.
17. Shapiro, S. L., A. J. Campillo, A. Lewis, G. J. Perreault, J. P. Spoonhower, R. K. Clayton, and W. Stoeckenius. 1978. Picosecond and steady state, variable intensity and variable temperature emission spectroscopy of bacteriorhodopsin. *Biophys. J.* 23:383–393.
18. Ippen, E. P., C. V. Shank, A. Lewis, and M. A. Marcus. 1978. Subpicosecond spectroscopy of bacteriorhodopsin. *Science* (*Wash. DC*). 200:1279–1281.
19. Shichida, Y., S. Matuoka, Y. Hidaka, and T. Yoshizawa. 1983. Absorption spectra of intermediates of bacteriorhodopsin measured by laser photolysis at room temperatures. *Biochim. Biophys. Acta.* 723:240–246.
20. Sharkov, A. V., Yu. A. Matveetz, S. V. Chekalin, A. V. Konyashchenko, O. M. Brekhov, and B. Yu. Rootskov. 1983. Fluorescence of bacteriorhodopsin under subpicosecond light excitation. *Photochem. Photobiol.* 38:108–111.
21. Oesterhelt, D., and W. Stoeckenius. 1974. Isolation of the cell membrane of *Halobacterium halobium* and its fractionation into red and purple membrane. *Methods Enzymol.* 31A:667–678.
22. Polland, H.-J., and W. Zinth. 1984. Generation of frequency shifted picosecond pulses with low temporal jitter. *Optics Commun.* 50:194–400.
23. Elsaesser, T., H.-J. Polland, A. Seilmeier, and W. Kaiser. 1984. Narrow-band infrared picosecond pulses tunable between 1.2 μm and 1.4 μm generated by a travelling-wave dye laser. *IEEE J. Quantum. Electron.* QE-20:191–194.
24. Polland, H.-J., and W. Zinth. 1985. A difference detection system for high-precision measurements of ultrafast transmission changes. *J. Phys. E. Sci: Instrum.* 18:399–400.
25. Oesterhelt, D., and L. Schuhmann. 1974. Reconstituion of bacteriorhodopsin. *FEBS* (*Fed. Eur. Biochem. Soc.*) *Lett.* 44:262–265.
26. Sens, B., and K. H. Drexhage. 1981. Fluorescence quantum yield of oxazine and carbazine laser dyes. *J. Lumin.* 24/25:709–742.
27. Lewis, A., J. P. Spoonhower, and G. J. Perreault. 1976. Observation of light emission from a rhodopsin. *Nature* (*Lond.*). 260:675–678.
28. Strickler, S. J., and R. A. Berg. 1962. Relationship between absorption intensity and fluorescence lifetime of molecules. *J. Chem. Phys.* 37:814–822.
29. Dinur, U., B. Honig, and M. Ottolenghi. 1981. Analysis of primary photochemical processes in bacteriorhodopsin. *Photochem. Photobiol.* 33:523–527.
30. Stockburger, M., W. Klusmann, H. Gattermann, G. Massig, and R. Peters. 1979. Photochemical cycle of bacteriorhodopsin studied by resonance Raman spectroscopy. *Biochemistry.* 18:4886–4900.
31. Aton, B., A. G. Doukas, R. H. Callender, B. Becher, and T. G. Ebrey. 1977. Resonance Raman studies of the purple membrane. *Biochemistry.* 16:2995–2999.
32. Alshuth, Th., and M. Stockburger. 1981. Structural changes in the retinal chromophore of bacteriorhodopsin studied by resonance Raman spectroscopy. *Ber. Bunsen-ges. Phys. Chem.* 85:484–489.
33. Goldschmidt, C. R., M. Ottolenghi, and R. Korenstein. 1976. On the primary quantum yields in the bacteriorhodopsin photocycle. *Biophys. J.* 16:839–843.
34. Hurley, J. B., and T. G. Ebrey. 1978. Energy transfer in the purple membrane of *Halobacterium halobium. Biophys. J.* 22:49–66.
35. Govindjee, R., T. G. Ebrey, and A. R. Crofts. 1980. The quantum efficiency of proton pumping by the purple membrane of *Halobacterium halobium. Biophys. J.* 30:231–242.
36. Becher, B., and T. G. Ebrey. 1977. The quantum efficiency for the photochemical conversion of the purple membrane protein. *Biophys. J.* 17:185–191.
37. Goldschmidt, C. R., O. Kalisky, T. Rosenfeld, and M. Ottolenghi. 1977. The quantum efficiency of the bacteriorhodopsin photocycle. *Biophys. J.* 17:179–183.
38. Oesterhelt, D., and B. Hess. 1973. Reversible photolysis of the purple complex in the purple membrane of *Halobacterium halobium. Eur. J. Biochem.* 37:316–326.
39. Oesterhelt, D., P. Hegemann, and J. Tittor. 1985. The photocycle of the chloride pump halorhodopsin. II. Quantum yields and a kinetic model. *EMBO* (*Eur. Mol. Biol. Organ.*) *J.* 4:2351–2356.
40. Casadio, R., H. Gutowitz, P. Mowery, M. Taylor, and W. Stoeckenius. 1980. Light-dark adaptation of bacteriorhodopsin in Triton-treated purple membrane. *Biochim. Biophys. Acta.* 590:13–23.
41. Kriebel, A. N., and A. C. Albrecht. 1976. Excitonic interaction among three chromophores: an application to the purple membrane of *Halobacterium halobium. J. Chem. Phys.* 65:4575–4583.
42. Ebrey, T. G., B. Becher, B. Mao, P. Kilbride, and B. Honig. 1977. Exciton interactions and chromophore orientation in the purple membrane. *J. Mol. Biol.* 112:377–397.
43. Schulten, K., and P. Tavan. 1978. A mechanism for the light-driven proton pump of *Halobacterium halobium. Nature* (*Lond.*). 272:85–86.
44. Schulten, K., Z. Schulten, and P. Tavan. 1984. An isomerization model for the pump cycle of bacteriorhodopsin. *In* Information and Energy Transduction in Biological Membranes. 10th. L. Bolis, E. J. M. Helmrich, and H. Passow, editors. Alan R. Liss., Inc., NY. 113–131.
45. Fang, J.-M., J. D. Carriker, V. Balogh-Nair, and K. Nakanishi. 1983. Evidence for the necessity of double-bond (13-Ene) isomerization in the proton pumping of bacteriorhodopsin. *J. Am. Chem. Soc.* 105:5162–5164.
46. Kölling, E., W. Gärtner, D. Oesterhelt, and L. Ernst. 1984. Sterically fixed retinal-analogue prevents proton-pumping activity in bacteriorhodopsin. *Angew. Chem. Int. Ed Engl.* 23:81–82.
47. Seilmeier, A., P. O. J. Scherer, and W. Kaiser. 1984. Ultrafast energy dissipation in solutions measured by a molecular thermometer. *Chem. Phys. Lett.* 105:140–146.
48. Birge, R. R., and T. M. Cooper. 1983. Energy storage in the primary step of the photocycle of bacteriorhodopsin. *Biophys. J.* 42:61–69.
49. Tavan, P., K. Schulten, and D. Oesterhelt. 1985. The effect of protonation and electrical interactions on the sterochemistry of retinal Schiff bases. *Biophys. J.* 47:415–430.
50. Smith, S. O., J. Lugtenburg, and R. A. Mathies. 1985. Determination of retinal chromophore structure in bacteriorhodopsin with resonance Raman spectroscopy. *J. Membr. Biol.* 85:95–109.
51. Tavan, P., and K. Schulten. 1986. Evidence for a 13,14-cis cycle in bacteriorhodopsin. *Biophys. J.* In press.
52. Nuss, M. C., W. Zinth, W. Kaiser, E. Kölling, and D. Oesterhelt. 1985. Femtosecond spectroscopy of the first events of the photochemical cycle in bacteriorhodopsin. *Chem. Phys. Lett.* 117:1–7.